Numerical Modeling of 1D Arterial Networks Coupled with a Lumped Parameters Description of the Heart

Luca Formaggia[a], Daniele Lamponi[b], Massimiliano Tuveri[c], Alessandro Veneziani[a]*

[a]MOX (Modeling and Scientific Computing), Dipartimento di Matematica "F. Brioschi",Politecnico di Milano,Via Bonardi 9, I - 20133 Milano, Italy

[b]CMCS, Ecole Polytechnique Federale de Lausanne, Ecublens, CH-1033 Lausanne, Switzerland

[c]Dipartimento di Chirurgia Generale e Vascolare, Clinica Sant'Elena, viale Marconi 160, 09045 Quartu Sant'Elena, Cagliari

The investigation on the pressure wave propagation along the arterial network and its relationships with vascular physiopathologies can be supported nowadays by numerical simulations (see e.g. [25]). One dimensional (1D) mathematical models, based on systems of two partial differential equations for each arterial segment suitably matched at bifurcations, can be simulated with low computational costs and provide useful insights into the role of wave reflections. For instance, those induced by the stiffening of the arterial walls or a vascular endoprosthesis, and their influence on the cardiac work. Some recent works have indeed moved in this direction ([19,6,25,24,33]).

The specific contribution of the present paper is to illustrate a 1D numerical model in which there is an effective coupling between the heart action and the 1D system. Often, the action of the heart on the arterial system is modelled as a boundary condition at the entrance of the aorta. However, it is well known that the left ventricle and the vascular network are a strongly coupled single mechanical system (see [15,23]). This coupling can be relevant in the numerical description of pressure waves propagation, particularly when dealing with pathological situations. In this work we propose a simple lumped parameter model for the heart and show how it can be coupled numerically with a 1D model for the arteries. Numerical results actually confirm the relevant impact of the heart-arteries coupling in realistic simulations.

1. Introduction

The aim of this paper is to investigate quantitatively the pressure wave propagation in the arterial tree by means of numerical models accounting for the coupling between the heart and the vascular system. We want to investigate different scenarios induced e.g. by ageing, by surgical operations and, in general, by a change of the mechanical characteristics of the arterial wall or the structure of the circulatory network.

Human arterial system can be mathematically described by different models with a different level of detail, from the ones based on the three-dimensional (3D) Navier-Stokes equations down to lumped parameters systemic representations based on the analogy between hydraulic and electric networks (see e.g. [8,20,9]). In particular, 1D models, originally introduced by Euler [4], seem to be appropriate for the study, in the time-space domain, of the pressure wave propagation induced by the fluid-wall interaction in the arterial tree (see e.g. [18,19,25,30,29,7,6]). For this reason they have already been adopted for the investigation of the relationships between anomalous "pressure wave" patterns and the presence of mechanical or geometrical modifications induced either by stenoses or by the presence of stents or prostheses (see [7,33]).

In this paper, we start from the arterial network model proposed in [34], where the 55 largest arteries are represented by 1D models suitably

*This work has been partially supported by EU RTN Haemodel Project (C.N. HPRN-CT-2002-00270), CNR Agenzia-2000 and FNS Project 20-100637/1. L. Formaggia, M. Tuveri and A. Veneziani gratefully acknowledge the Bernoulli Institute of EPFL, Lausanne, for hosting them and provide a fruitful working environment that helped finalising this work.

matched at the bifurcations. The parameters specifying the mechanical and physical features of each vessel have been taken by [35] and [28] and later adjusted by Wang and Parker in [34]. The remaining part of the arterial tree (peripheral circulation) has been modelled by a terminal impedance modelled on a three-elements Windkessel lumped parameter model.

Normally, the action of the heart is represented by a boundary condition to be prescribed at the inlet of the first artery of the network, i.e. the aorta. However, it is well known that "the left ventricle and arterial circulation represent two mechanical units that are joined together to form a coupled biological system" [15, Chap.13]. The relevance of the heart-arterial interaction in mathematical modelling has been pointed out in [23,22], in the framework of lumped parameter models. The reduction of the heart action to a boundary condition for the system does not account at all for this coupling. This approach is unsatisfactory in particular when we want to study the effect on the pressure and flow patterns caused by changes in the geometrical or mechanical characteristics of the arterial network. No feedback from the arterial tree to the heart is indeed being modelled in this way. In this work, we propose to overcome this drawback by a coupled description based on the matching of the 1D network model with a lumped parameter model for the left ventricle. In particular, we refer to the model illustrated in [15] and in [5], together with a technique that accounts for the closure of the aortic valve. A representation of the proposed model is in Fig.1.

We have used the model to simulate the physiological characteristics of individuals of different age. In fact, arterial stiffness increases with age and this reflects in a change of the pulse wave pattern. In particular, we have investigated the overload on the heart induced by the backward travelling waves, whose relevance is increased by the stiffening of the walls. In a similar way, some pathological situations can be considered, where anomalous pressure wave reflections could have some consequences on the heart. Abrupt changes in the compliance of a particular district, induced for instance by the presence of an endoprosthesis,

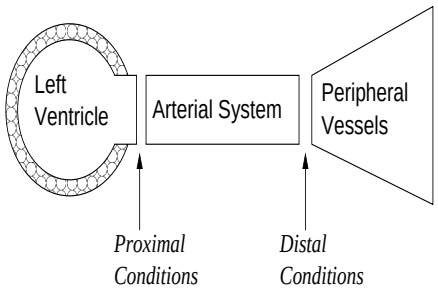

Figure 1. Representation of the simulated system. The arterial network is described in terms of 1D models, while the heart and the peripheral circulation are given by lumped parameters models.

can still be described at the mathematical level with an appropriate modification of the physical parameters of the 1D network. Drastic modification in the arterial network such as the ones induced by an amputation can be described as well as by modifying the arterial network accordingly. Preliminary numerical results referring to such pathological cases are presented here.

The outline of the paper is as follows. Sect. 2 and 3 are the "*Materials and Methods*" sections of the paper, where we detail the proposed model. More precisely, in Sect. 2 we introduce the mathematical model while in Sect. 3 we describe the numerical techniques used for the numerical simulation. In particular we address the coupling between arterial and heart models. In the "*Results*" Sect. 4 we define the numerical test cases and present the obtained results, that are extensively discussed in Sect. 5. Conclusions and future developments are drawn in Sect. 5.1.

2. The Mathematical Model

The basic 1D model is derived for a single artery approximated as a straight cylinder. More details are found, for instance, in [20]. We obtain a system of two partial differential equations describing the evolution of the vessel section area A

and the mass flux Q along the vessel axis, and, as a consequence, of the mean pressure P. Indeed the latter is taken to be linked to the vessel radius (and thus A) by a relation derived by the mechanics of the vessel wall structure. We will make use of a full non-linear model, since the non linear wave interactions are of importance (see [19]).

Since the human arterial system is formed by a network of vessels we need to find a proper way to account for branching. We address this issue in Sect. 2.1.2.

Finally, the model is completed by accounting of the peripheral circulation and the heart. The former will be regarded as a boundary condition for the 1D network distal sections. As pointed out in Sect. 1, also the heart could be described as a boundary condition for the proximal section of the 1D model. We will show how this approach is not suitable to investigate the effect at the level of aortic pressure for changes of the network characteristics. An alternative approach is thus advocated, which consists in modelling also the heart action through a differential equation (Sect. 2.3).

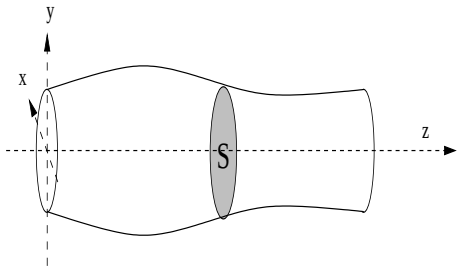

Figure 2. The cylindrical domain Ω_t. The cylinder axis is aligned with the coordinate z. We assume that the axial sections z =const. remain circular at all times.

2.1. One-dimensional model of the arterial network

2.1.1. The basic one dimensional model

The starting point are the Navier Stokes equations, which govern blood flow in large and medium sized arteries, where the approximation of Newtonian rheology is commonly accepted. The equations are posed in a cylindrical domain Ω of length L, as depicted in Fig. 2. The domain changes in time because of the flow induced wall movement, and we assume that the vessel displaces only in the radial direction and the flow is axi-symmetric. The pressure P is taken to be constant on each axial section $S = S(z,t)$ and we assume that viscous effects are relevant only near the wall boundary. We further postulate that the velocity component along the vessel axis, u_z, is dominant with respect to the other components.

After integrating the Navier-Stokes equation over a generic axial section we obtain the following system of two partial differential equations,

$$\frac{\partial A}{\partial t} + \frac{\partial Q}{\partial z} = 0 \qquad (1)$$

$$\frac{\partial Q}{\partial t} + \frac{\partial}{\partial z}\left(\alpha \frac{Q^2}{A}\right) + \frac{A}{\rho}\frac{\partial P}{\partial z} + K_R \frac{Q}{A} = 0 \qquad (2)$$

for all $z \in (0, L)$ and $t > 0$, where the unknowns A, Q and P denote the section area, averaged volume flux and mean pressure, respectively, and they are defined as

$$\begin{aligned} A(z,t) &= \int_{S(z,t)} dy\, dz, \\ Q(z,t) &= \textstyle\int_{S(z,t)} u_z(x,y,z,t) dx\, dy = A\overline{u}, \\ P(z,t) &= (A(z,t))^{-1} \int_{S(z,t)} P(x,y,z,t) dy\, dz. \end{aligned} \qquad (3)$$

Here K_R is a resistance parameter related to the viscosity of blood, taken equal to $8\pi\nu$ (the value that corresponds to a parabolic velocity profile) and α is the momentum correction coefficient $\alpha = (\int_S u_z^2 d\gamma)/A\overline{u}^2$, which for a parabolic profile would be equal to 4/3. Yet, following the arguments in [27] we have here taken directly $\alpha = 1$, a value which also leads to several mathematical simplifications [20].

System (1), (2) is closed by a relation for the pressure P derived from a mechanical model for the vessel wall displacement. For instance, by

assuming instantaneous equilibrium by Laplace law we derive

$$P - P_{ext} = \beta_0 \frac{\sqrt{A} - \sqrt{A_0}}{A_0}, \quad \beta_0 = E h_0 \sqrt{\pi}, \quad (4)$$

where h_0 is the wall thickness at the reference configuration. β is in general a function of z through the Young modulus E. Other relations may be adopted as well (see e.g. [16]) and we refer to [20] for a more thorough discussion and analysis. In this work we have always used relation (4), and we also set (without loss of generality) $P_{ext} = 0$. The quantity

$$c_1 = \sqrt{\frac{A}{\rho}\frac{\partial P}{\partial A}} = \sqrt{\frac{\beta_0}{2\rho A_0}} A^{\frac{1}{4}} \quad (5)$$

represents the speed of pulse waves relative to blood flow. One immediately recognises that whenever β_0/A_0 increases, either because of a rise in the Young modulus (stiffening of the arteries) or because A_0 is decreasing (tapering), we have an acceleration of the pulse waves.

We assume that the initial time is $t = 0$, and we prescribe suitable initial conditions for A and Q, respectively. Boundary conditions need to be assigned as well. Their prescription will be discussed in the next Sections.

The mathematical analysis of this system outlines its hyperbolic nature (see [20]). The solution is the non-linear super-imposition of two simple waves, travelling in opposite directions with a velocity given by

$$\lambda_{1,2} = \frac{Q}{A} \pm c_1, \quad (6)$$

respectively. The piece of information carried out by each simple wave is made up by a special combination of mass flux and pressure, the so called *Riemann invariants* W_i $i = 1, 2$ (also called *characteristic variables* - see e.g. [19]). The actual expression of the Riemann invariants (see e.g. [20]) is obtained by fixing a reference state. The choice of the rest conditions ($A = A_0, Q = 0$) as the reference state yields

$$W_{1,2} = \frac{Q}{A} \pm 4\sqrt{\frac{\beta_0}{2\rho A_0}}(A^{\frac{1}{4}} - A_0^{\frac{1}{4}}) = \overline{u} \pm 4(c_1 - c_{1,0}), \quad (7)$$

where $c_{1,0}$ corresponds to the speed of the pulse wave in (5) when $A = A_0$. Relations (7) can be inverted, leading to

$$\begin{cases} A = \left(\frac{2\rho A_0}{\beta}\right)^2 \left(\frac{W_1 - W_2}{8} + c_{1,0}\right)^4, \\ Q = A\frac{W_1 + W_2}{2}. \end{cases} \quad (8)$$

These relations play an important role for the imposition of boundary conditions.

Boundary conditions on a cylindrical domain

Before addressing the network modelling, it is worthwhile to remind some basic facts in the boundary treatment of hyperbolic problems, referring to the single artery case (see Fig. 3). As for the typical values of $\overline{u}$ and c_1 in blood flow the two simple waves travel always in opposite directions, on each boundary point we may specify only a single boundary condition (see e.g. [21]).

In the domain Ω of Fig. 3 at boundaries Γ_1 and Γ_2 we would like to prescribe conditions which correctly account for the wave propagation. For instance, the single wave propagating from the left to right should exit boundary Γ_2 without any backward reflection. A perfectly *non-reflecting* boundary condition would thus force a null backward wave, i.e. $W_2 = 0$ on Γ_2. In more general situations, a non-reflecting condition prescribes only the piece of information associated to the entering wave. If the z coordinate local to each artery is oriented in the proximal-to-distal direction, at the proximal boundary the entering simple-wave is associated to W_1, while W_2 enters at the distal end. This means that non-reflecting conditions are of the form

$$W_1(A, Q) = g_1(t), \text{ on } \Gamma_1 \quad (9)$$

$$W_2(A, Q) = g_2(t), \text{ on } \Gamma_2, \quad (10)$$

g_1 and g_2 being given functions.

2.1.2. Modelling of bifurcations

The arterial system is characterised by the presence of branching. Bifurcations and their mathematical modelling are the subject of many

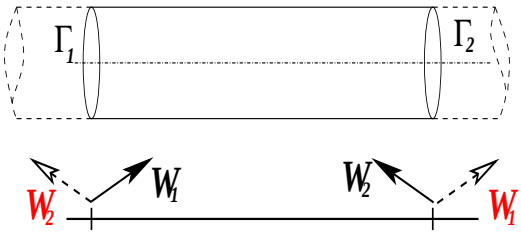

Figure 3. One dimensional model with non-reflecting conditions.

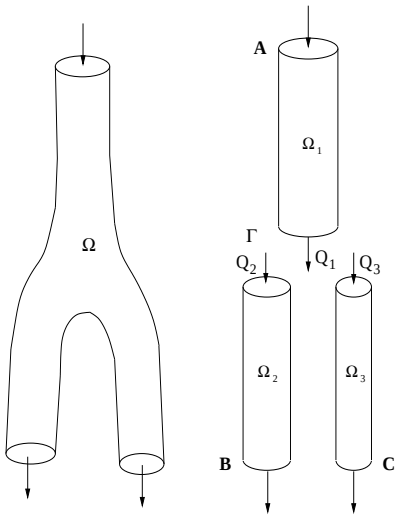

Figure 4. One dimensional model of bifurcation by domain decomposition technique.

recent studies (see [26,27,6]). In fact, the accuracy by which the mathematical models describe major bifurcations is of utmost importance for a correct simulation of pressure wave propagation and reflection. Here we have taken a simple approach that ensures the conservation of mass flux and total pressure. More precisely, in order to solve the three problems in Ω_1 (main branch), Ω_2 and Ω_3 (sibling vessels) of Fig. 4 we impose

$$\begin{cases} Q_1 - Q_2 - Q_3 = 0 \\ P_{t,1} = P_{t,2} = P_{t,3}, \end{cases} \qquad \text{at } \Gamma, t > 0, \quad (11)$$

where $P_t = P + \frac{\rho}{2}\left(\frac{Q}{A}\right)^2$, and Γ is the branching point. Since in each branch we are dealing with a hyperbolic system, these three conditions are sufficient to close the problem at the differential level. Moreover, conditions (11) are compatible with global energy decay for the associated nonlinear system [6].

A potentially more accurate description of the bifurcation that accounts for the angle among the branches has been proposed in [6]. Numerical evidence suggests however that at a quantitative level, at least for the purposes of the present work, the differences with respect the results obtained with (11) are negligible.

2.2. Boundary conditions for the network

Boundary conditions are either distal or proximal. The former has to simulate in a simplified way the presence of the capillary bed. The latter, which is imposed at the proximal node in the ascending aorta, accounts for the action of the heart (or, more precisely, of the left ventricle).

2.2.1. Distal conditions (peripheral circulation)

At the distal ends a common choice is to assume that the peripheral circulation corresponds to a purely resistive load (see e.g. [25]). This corresponds to assume that

$$p_d = R_p Q_d. \quad (12)$$

When resorting to non reflecting boundary conditions reformulated in terms of Riemann invariants, we can linearise system (7) in the form

$$W_1 = a_1 Q + a_2 p, \quad W_2 = a_1 Q - a_2 p$$

where a_1 and a_2 are assumed to be constant. Condition (12) can be therefore rewritten as

$$\frac{W_1 - W_2}{2a_2} = R_p \frac{W_1 + W_2}{2a_1}.$$

After trivial manipulation, we obtain

$$W_2 = -\frac{a_1 - \frac{a_2}{R_p}}{a_1 + \frac{a_2}{R_p}} W_1 = -R_T W_1 \tag{13}$$

where we have set $R_T = \left(a_1 - \frac{a_2}{R_p}\right) / \left(a_1 + \frac{a_2}{R_p}\right)$. This condition states in an immediate way that the back propagating Riemann invariant is (up to the sign) a fraction of the incoming one (see e.g. [25]). Observe, in particular, that if if R_p tends to infinity, that means condition (12) corresponds to a completely blocked end ($Q_p = 0$), R_T tends to 1, as expected.

The hypothesis that the peripheral circulation can be represented in terms of a resistive impedance is correct for very peripheral vessels. Our model will be used for simulating different scenarios, considering different possible distal boundaries. We therefore generalise previous condition when the lumped parameter representation of the peripheral circulation is given by a complex impedance Z_p. In particular, if we consider the *three-element Windkessel model* represented in Fig. 5, the *input impedance* is

$$Z_p = R_0 + \frac{R_1}{1 + i\omega R_1 C}.$$

Modulus and phase of this impedance are illustrated in Fig. 6. In the time domain, by setting $R_0 + R_1 = R_p$, we have the following generalisation of the resistive condition (12)

$$p + R_1 C \frac{dp}{dt} = R_p Q + R_0 R_1 C \frac{dQ}{dt}. \tag{14}$$

When resorting to the (linearised) Riemann invariants, after some manipulations, condition (14) reads

$$\begin{aligned} R_1 C \frac{a_2 + \frac{a_1}{R_0}}{a_2 + \frac{a_1}{R_p}} \frac{dW_2}{dt} + W_2 = \\ R_1 C \frac{a_2 - \frac{a_1}{R_0}}{a_2 + \frac{a_1}{R_p}} \frac{dW_1}{dt} - \frac{a_2 - \frac{a_1}{R_p}}{a_2 + \frac{a_1}{R_p}} W_1. \end{aligned} \tag{15}$$

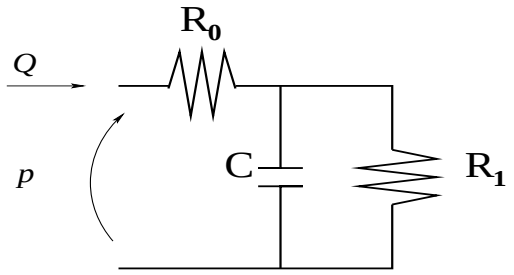

Figure 5. Three-elements Windkessel model used for modelling the peripheral circulation.

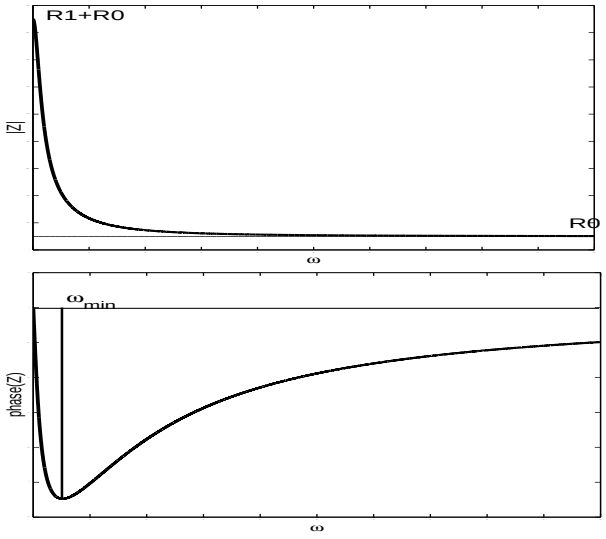

Figure 6. Impedance of the three-elements Windkessel model: modulus (top) and phase (bottom).

Time integration of (15) (pursued at the numerical level, as described in Sect. 3) provides the distal boundary conditions.

Observe that if we suppose that R_0 tends to infinity (corresponding to a complete occlusion of the peripheral boundary), if the initial data are compatible (i.e. $Q_P = 0$ at the initial time) it is possible to verify that we obtain $Q_P = 0$ at any time, as expected.

2.2.2. Proximal Conditions: Standard model

At the inlet we need to simulate the presence of the heart and of the aortic valve. Proximal boundary conditions may be further subdivided into two types: *open valve condition* (OV) and *closed valve conditions* (CV). The change in condition type is driven by the solution itself. For the sake of simplicity, we detail here OV and CV separately. How is it possible to switch between the states in the numerical model is explained in Sect. 3.4.

CV Conditions: When the valve is closed the boundary condition imposed at a given instant at the proximal aortic node is $Q = 0$. In practise we resort to a condition similar to (13), where now the roles of W_1 and W_2 are exchanged and $R_T = 1$, yielding to

$$W_{1,CV} = -W_2. \tag{16}$$

OV Conditions: In this situation a classical methodology is to prescribe the flux or the pressure at the proximal node using a well chosen profile. We should note however that prescribing pressure or fluxes is a reflective-type condition. This means that *part of the wave going toward the heart will be reflected back into the network.* If this is what we expect when the aortic valve is closed, it may otherwise give unwanted spurious waves in the case of OV conditions, since we are not accounting for the absorbing properties of the ventricle. Smoother results are obtained using a non-reflecting boundary condition, by imposing the incoming Riemann invariant W_1 instead, obtained from the profile of the ventricular pressure P_v. Namely, the incoming Riemann invariant W_1 is written in terms of the pressure and W_2 as it follows,

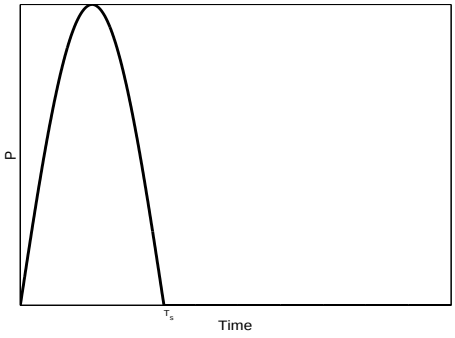

Figure 7. Function $P_{v,0}(t)$ for the left-ventricle pressure P_V in the case of standard boundary conditions. $T_S = 0.3$s is the end-of-systole time.

$$W_1 = W_2 + 4\sqrt{\frac{2}{\rho}}\left(P_v + \frac{\beta}{\sqrt{A_0}}\right). \tag{17}$$

In practise, P_v has been chosen as an half sinus of amplitude $P_{v,0}$ and a half-period $t_v = 0.3$s (see Fig. 7); the profile will be restarted at every heart beat (we will indicate the heart beat period by T). If we assume that the ventricle acts as a perfectly absorbing chamber, the value of W_2 must remain unchanged and equal to its initial value $W_{2,0}$, readily computed from the initial state at the aortic proximal node. In the general case, the actual value of W_2 is computed by extrapolation (see Sect. 3).

With this method we will not impose the pressure P_v exactly at the proximal node, since we are selecting just the piece of information corresponding to the wave entering the network. However, we are now sure that the waves coming from the periphery will be perfectly absorbed. As previously pointed out, this approach does not account at all of the behaviour of the heart and of the coupling between the left ventricle and the arterial system, since P_v is given.

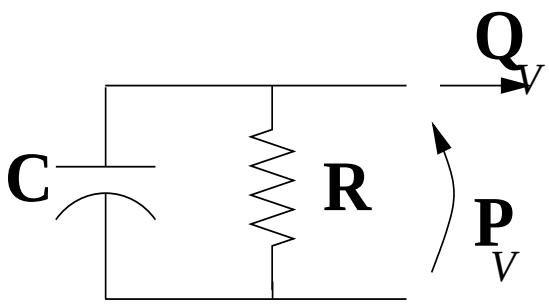

Figure 8. Lumped parameters representation of the heart during the systolic phase.

2.3. Lumped parameters description of the heart

We describe here an alternative technique, based on a commonly accepted phenomenological model of the ventricle function. The basic idea of this model, originally proposed in [32,31] (see also [15,5,11,23]) is that the pressure in the left ventricle and the ventricular volume are linked through a time-dependent coefficient called *elastance*. In particular, the cardiac elastance is low during the diastole and increases in systole. In [32,31] it is experimentally shown that the elastance function is in fact independent of the ventricular load. We will therefore assumed that the ventricle pressure P_v and the ventricular volume V_v are linked by the following relation,

$$\begin{aligned} P_v(t) &= E_v(t)(V_v(t) - V_0) + KE_v(t)(V_v - V_0) \\ &\times Q_v(t) = E_v(t)(V_v(t) - V_0)(1 + KQ_v(t)) \end{aligned} \tag{18}$$

Here $E_v = E_v(t)$ is a time varying elastance that simulates the action of the heart muscular fibres, V_0 is a reference volume and K is a resistance coefficient (see [15, Chap.13, eq. (13.4)]). E_v, K and V_0 are intrinsic properties of the ventricle. K is usually rather small, so in a first it may be set to zero. We also assume that V_0 is constant. Observe that the flow rate ejected by the ventricle is given by $Q_V = -dV_V/dt$. During systole, when the atrio-ventricular valve is closed, equation (18) is matched with the 1D network (*OV conditions*). More precisely, a differential expression is obtained by deriving in time of (18),

$$\frac{1}{E}\frac{dP_V}{dt} + \frac{d}{dt}\left(\frac{1}{E}\right)P_V = \frac{dV}{dt} = -Q_V,$$

whose electrical analogue is illustrated in Fig. 8.

The presence of the venous system, which is responsible of the pressure increment in the heart during the diastole, is not considered in an explicit way, since we are simulating here just the left ventricle action. This means that (18) is restarted at the beginning of each systolic cycle (more precisely at the start of the isochoric contraction), when we impose the volume of blood in the ventricle.

Referring to the electrical analogy, this corresponds to a re-polarisation of the capacitor in Fig. 8. The systolic phase will then coincides with the depolarisation of the capacitor, yielding the blood ejection into the arterial system.

3. Numerical methods

3.1. Discretisation of a single artery

We discretized system (1, 2) using a second order (explicit) Taylor-Galerkin Finite Element scheme [3,1]. This numerical scheme is well suited to wave propagation problem as it has a good phase accuracy for a large range of wave numbers. Details may be found in [20].

Each arterial segment of the network, Ω_i, is subdivided into a number of finite elements of size h_i. For the sake of simplicity we have kept h_i constant on each artery, while it may vary between arteries. Time is advanced using a time step Δt that has to satisfy a CFL stability condition stating that the ratio $\frac{h_i}{\Delta t}$ should be everywhere greater than a given fraction ($\sqrt{3}$ in our case) of the maximum wave speed $c_1 + Q/A$. Since the wave speed is a function of the solution, Δt should be adjusted during the computation. However, for blood flow problems it is not difficult to estimate a reasonable upper bound for the wave speed and thus guarantee a-priori that the chosen Δt will always be within the stability range.

In each arterial segment the scheme provides the equations that link the approximation at time t^n to that at time t^{n+1} at the interior finite element nodes. The values at the boundary and at the branching points are obtained as explained in the next section. The approximation at time $t^0 = 0$ is computed from the given initial values.

Generalities on the imposition of the boundary conditions

We have seen that the hyperbolic nature of the problem implies that one boundary (or integral) condition has to be imposed at each end. Yet, at numerical level, we have to provide at the boundary nodes two pieces of information at each time step t^{n+1}: the value of A^{n+1} and Q^{n+1}. To exemplify the techniques used to build the missing datum, consider a distal boundary and assume that the boundary condition is given in the form

$$W_2(A^{n+1}, Q^{n+1}) = g_2(t^{n+1}). \tag{19}$$

The first Riemann invariant is associated to the wave that leaves the domain through the distal node travelling at speed λ_1. In the absence of source terms W_1 satisfies the equation

$$\frac{\partial W_1}{\partial t} + \lambda_1 \frac{\partial W_1}{\partial x} = 0$$

and, therefore, is constant along the characteristics curve $dx/dt = \lambda_1(A(t), Q(t)$ [10]. If $z = L$ is the coordinate of the distal node, we can write the following approximation for W_1^{n+1} in (22)

$$W_1^{n+1} = W_1(t^n, L - \lambda_1^n \Delta t) =: W_{1,\text{ext}}^{n+1}, \tag{20}$$

a technique also known *as extrapolation of the outgoing Riemann invariant.* If we have a source term, the procedure is still applicable with some minor modifications (see [20]).

We may note that, as a consequence of the stability limitation on Δt, the point $x = L - \lambda_1^n \Delta t$ falls necessarily inside the mesh element adjacent to the distal node. Consequently, $W_{1,\text{ext}}^{n+1}$ may be readily computed by interpolating between the values at the two last mesh nodes.

The extrapolation of W_1 and the prescription of W_2 give now all the data sufficient to solve the numerical problem. Indeed, we may compute the boundary values for A and Q at the distal node by solving the non linear system

$$\begin{cases} W_1(A^{n+1}, Q^{n+1}) = W_{1,\text{ext}}^{n+1} \\ W_2(A^{n+1}, Q^{n+1}) = g_2. \end{cases} \tag{21}$$

Similar considerations can be carried out on the proximal node, where the incoming W_1 is prescribed and the outgoing W_2 can be extrapolated along the characteristic curve driven by the eigenvalue λ_2.

3.1.1. Branching conditions

The extrapolation of the outgoing Riemann invariant can be used also for the branching conditions. Let us consider Figure 4. The systems provided by the Taylor-Galerkin scheme for each artery has to be complemented by six relations for the unknowns A_i^{n+1}, Q_i^{n+1}, $i = 1, 2, 3$ at the bifurcation point. By exploiting relations (11) and the extrapolation of the outgoing characteristics (W_1 for Ω_1, W_2 for Ω_2 and Ω_3) we can build, at each time step, a non linear system for the desired quantities. The system can be solved numerically with a few iterations of a Newton-Raphson procedure.

3.2. Peripheral circulation

At numerical level, relation (15) provides an equation for the approximation at time t^{n+1} of W_1 and W_2 at a distal boundaries. More precisely, for the sake of notation we set

$$s_1 = R_1 C \frac{a_2 + \frac{a_1}{R_0}}{a_2 + \frac{a_1}{R_p}}, \quad s_2 = R_1 C \frac{a_2 - \frac{a_1}{R_0}}{a_2 + \frac{a_1}{R_p}},$$
$$s_3 = \frac{a_2 - \frac{a_1}{R_p}}{a_2 + \frac{a_1}{R_p}}.$$

If we discretized (15) with a backward Euler scheme, we obtain the equation

$$W_2^{n+1} = \frac{(s_2 - \Delta t s_3) W_1^{n+1} + s_1 W_2^n - s_2 W_1^n}{\Delta t + s_1}. \tag{22}$$

As before, this relation is completed by the extrapolation of the outgoing characteristic. Which is also needed by the fact that the right hand side

of (22) depends on W_1^{n+1}. We therefore obtain the non linear system

$$\begin{cases} W_1(A^{n+1}, Q^{n+1}) = W_{1,\text{ext}}^{n+1} \\ \\ W_2(A^{n+1}, Q^{n+1}) = \\ \qquad \dfrac{(s_2 - \Delta t s_3) W_1^{n+1} + s_1 W_2^n - s_2 W_1^n}{\Delta t + s_1}, \end{cases} \tag{23}$$

still to be solved with a Newton scheme.

3.3. Proximal boundary

3.3.1. Standard conditions

In this case, the boundary condition we prescribe is the incoming Riemann variable W_1 through equation (16) when the aortic valve is closed or (17) when it is open. The other condition is obtained by extrapolating W_2.

In the case of CV conditions, we will therefore set:

$$W_2^{n+1} = W_{2,ext}^{n+1}, W_1^{n+1} = -W_2^{n+1} = -W_{2,ext}^{n+1}. \tag{24}$$

In the case of OV conditions, having prescribed a ventricular pressure function $P_v(t)$, we will force:

$$\begin{aligned} W_1^{n+1} &= W_{2,\text{ext}}^{n+1} + 4\sqrt{\frac{2}{\rho}} \left(P_v(t^{n+1}) + \tfrac{\beta}{\sqrt{A_0}} \right) \\ W_2^{n+1} &= W_{2,\text{ext}}^{n+1}, \end{aligned} \tag{25}$$

3.3.2. Heart model

When accounting for a lumped parameters description of the heart, conditions (24) are still valid in the case of CV.

For what concerns OV conditions, given the quantities at time t^n, we approximate (18) to obtain the pressure at time t^{n+1} as it follows

$$\begin{aligned} P_v^{n+1} = E(t^{n+1}) \left(V_v^n - \frac{Q_v^{n+1} + Q_v^n}{2} \Delta t - V_0 \right) \\ + R(t^n, V_v^n) Q_v^{n+1}, \end{aligned} \tag{26}$$

where V_v^n is the ventricular volume at $t = t^n$. We assume that when the aortic valve is open the values of P_a and Q_a at the proximal aortic node coincide with P_v and Q_v, respectively.

Equation (26) and the extrapolation of W_2 are the boundary conditions for the open valve case. We can then update the ventricular volume as $V_v^{n+1} = V_v^n - \frac{Q^{n+1}+Q^n}{2}\Delta t$.

To simulate the cardiac cycle, we re-activate the model at each time $t^* = kT$, $k = 0, 1, \ldots$, being T the chosen beat period. At these times we assume that the ventricle is completely filled with $V_v(t^*) = V^*$ being the chosen stroke volume, while $E(t^*)$ corresponds to its lowest value (end diastole). While the aortic valve opens (see next subsection for the modelling of the valve) we have $Q_v^n = Q_v^{n+1} = 0$ and $V_v^n = V^*$ (isochoric contraction) and (26) is sufficient to compute P_v^{n+1}. Until the aortic valve remains closed, the ventricular model is completely decoupled from the network model and the proximal boundary condition for the latter is determined by the zero flux condition.

3.4. Aortic valve action

We have assumed that the valve opens under the action of a differential pressure, while it closes under the action of a flow reversal.

The diastolic cycle is started with the valve closed and at each time step P_v^{n+1} is compared to that P_a^{n+1}, the pressure computed by the 1D model at the aortic proximal node. When $P_v^{n+1} - P_a^{n+1} > 0$ the aortic valve is opened and from the successive time step onward we adopt the OV conditions, until the next closure.

Clearly, when the valve opens at the end of the isochoric contraction the ventricular pressure is still rapidly increasing and induces a positive flux into the aorta. To determine the instant of valve closure (end systole) we monitor the sign of the flux at the aortic proximal node. At the first time step when we have $Q_v^{n+1} < 0$ we "close" the valve by adopting again the CV boundary condition, until the next heart cycle. A flow chart representation of the aortic valve action is given in Fig.9.

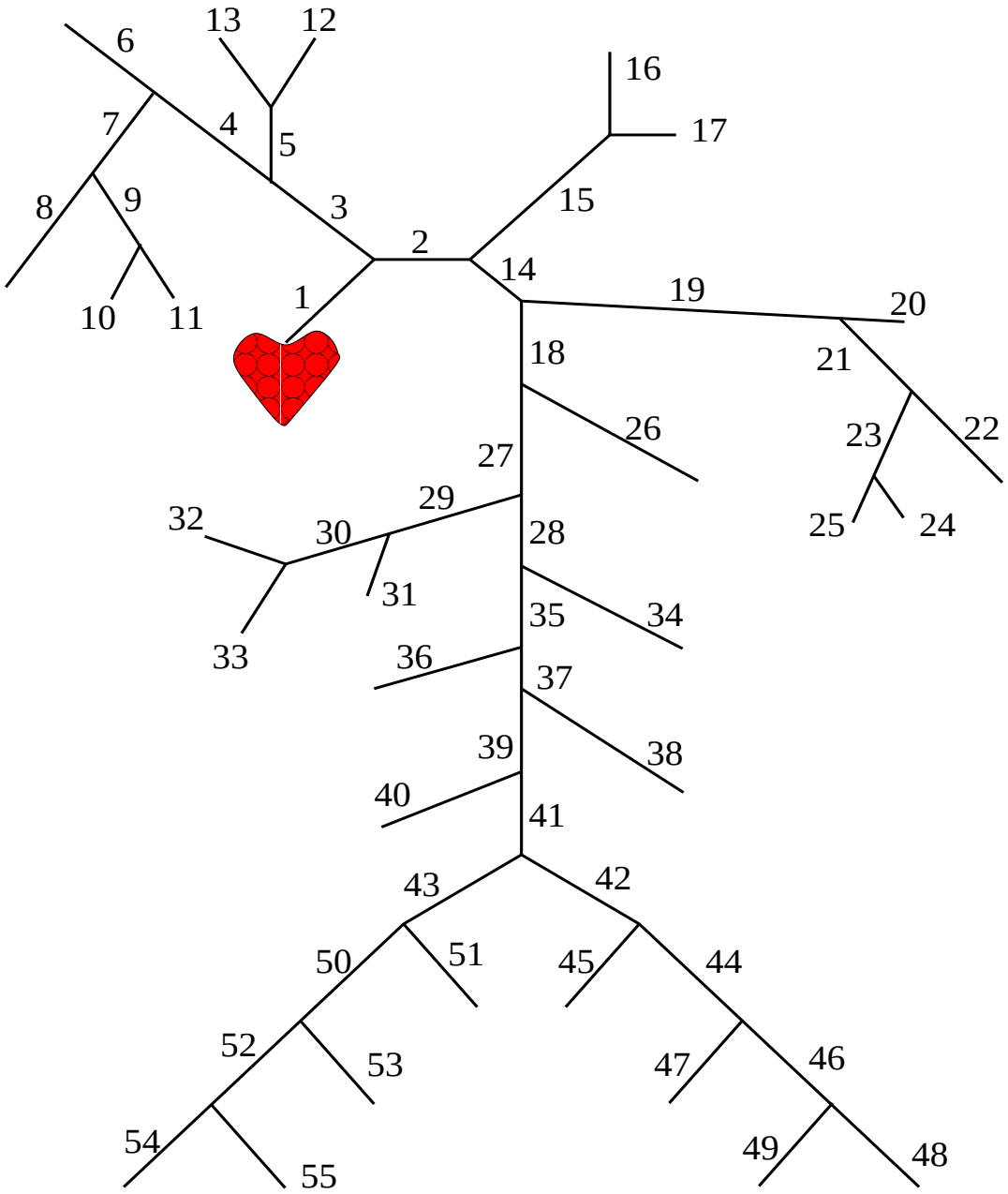

Figure 10. Arterial tree composed of a set of 55 straight vessels, described by 1D models. Physiological case (see [34]).

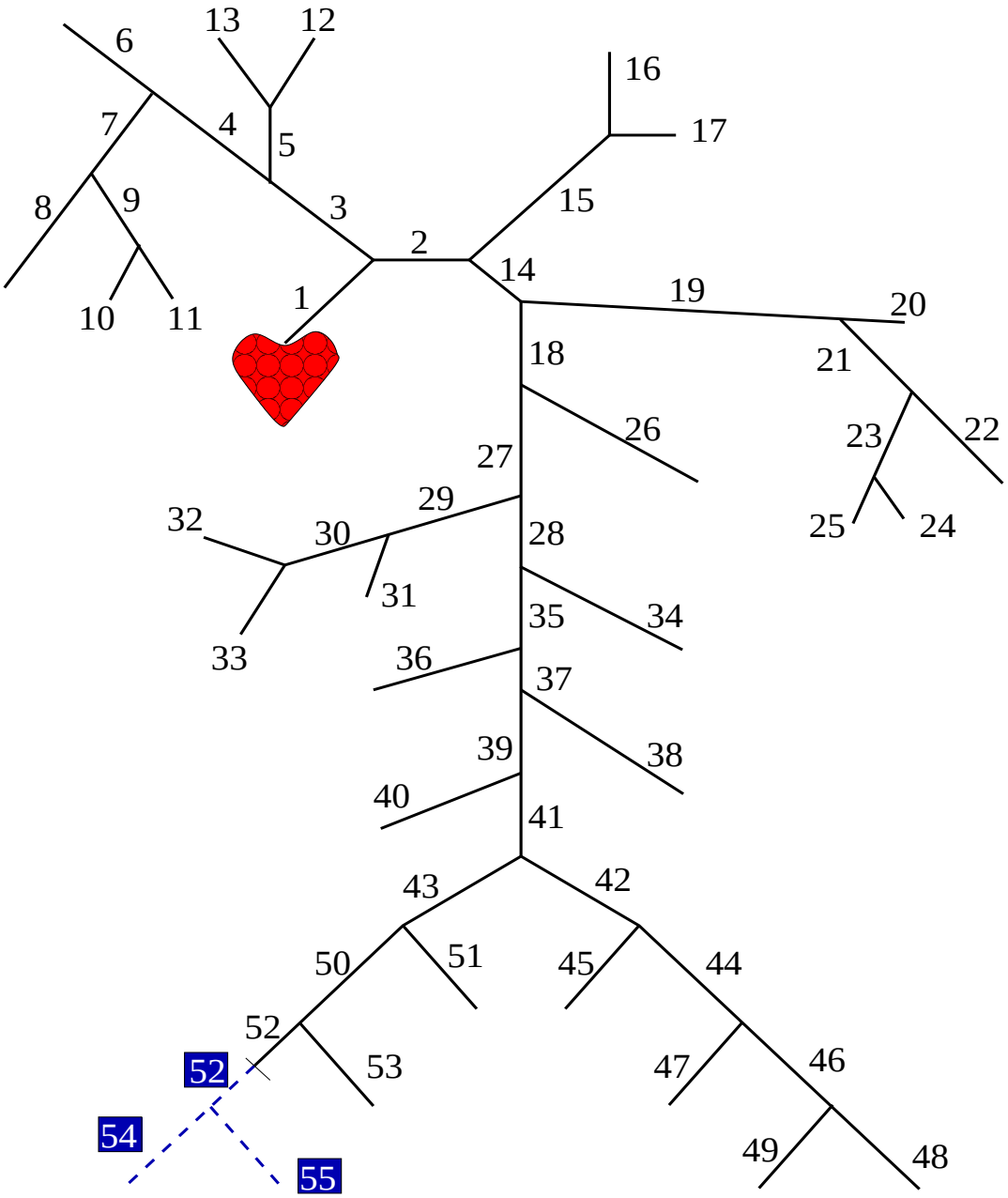

Figure 11. Arterial tree composed of a set of 55 straight vessels, described by 1D models. Pathological test case: vessels outlined in the boxes are cut away from the system.

#	Name of Artery	Length (cm) -	Area (cm^2) -	Beta (β) (kg/s^2)	Reflection coefficient (R_t) -
1	Ascending Aorta	4.0	5.983	388	-
2	Aortic Arch I	2.0	5.147	348	-
3	Brachiocephalic	3.4	1.219	932	-
4	R. Subclavian I	3.4	0.562	1692	-
5	R. Carotid	17.7	0.432	2064	-
6	R. Vertebral	14.8	0.123	10360	0.906
7	R. Subclavian II	42.2	0.510	1864	-
8	R. radial	23.5	0.106	11464	0.82
9	R. Ulnar I	6.7	0.145	8984	-
10	R. Interosseous	7.9	0.031	51576	0.956
11	R. Ulnar II	17.1	0.133	9784	0.893
12	R. internal Carotid	17.6	0.121	10576	0.784
13	R. external Carotid	17.7	0.121	9868	0.79
14	Aortic Arch II	3.9	3.142	520	-
15	L. Carotid	20.8	0.430	2076	-
16	L. internal Carotid	17.6	0.121	10576	0.784
17	L. external Carotid	17.7	0.121	9868	0.791
18	Thoracic Aorta I	5.2	3.142	496	-
19	L. Subclavian I	3.4	0.562	1664	-
20	Vertebral	14.8	0.123	10360	0.906
21	L. Subclavian II	42.2	0.510	1864	-
22	L. Radial	23.5	0.106	11464	0.821
23	L. Ulnar I	6.7	0.145	8984	-
24	L. Interosseous	7.9	0.031	51576	0.956
25	L. Ulnar II	17.1	0.133	9784	0.893
26	Intercostals	8.0	0.196	3540	0.627
27	Thoracic Aorta II	10.4	3.017	468	-
28	Abdominal I	5.3	1.911	668	-
29	Celiac I	2.0	0.478	1900	-
30	Celiac II	1.0	0.126	7220	-
31	Hepatic	6.6	0.152	4568	0.925
32	Gastric	7.1	0.102	6268	0.921
33	Splenic	6.3	0.238	3224	0.93
34	Superior Mesenteric	5.9	0.430	2276	0.934
35	Abdominal II	1.0	1.247	908	-
36	L. Renal	3.2	0.332	2264	0.861
37	Abdominal III	1.0	1.021	1112	-
38	R. Renal	3.2	0.159	4724	0.861
39	Abdominal IV	10.6	0.697	1524	-
40	Inferior Mesenteric	5.0	0.080	7580	0.918
41	Abdominal V	1.0	0.578	1596	-
42	R. common Iliac	5.9	0.328	2596	-
43	L. common Iliac	5.8	0.328	2596	-
44	L. external iliac	14.4	0.252	5972	-
45	L. internal Iliac	5.0	0.181	12536	0.925
46	L. Femoral	44.3	0.139	10236	-
47	L. deep Femoral	12.6	0.126	10608	0.885
48	L. posterior Tibial	32.1	0.110	23232	0.724
49	L. anterior Tibial	34.3	0.060	36972	0.716
50	R. external Iliac	14.5	0.252	5972	-
51	R. internal Iliac	5.1	0.181	12536	0.925
52	R. Femoral	44.4	0.139	10236	-
53	R. deep Femoral	12.7	0.126	10608	0.888
54	L. posterior Tibial	32.3	0.110	23232	0.724
55	R. anterior Tibial	34.4	0.060	36972	0.716

Table 1
Data used in the computational model of the 55 arteries. The data is from the physiological data published in [35] and [28] with the changes made in [34] and has been normalised with respect to the area of the ascending aorta (artery 1).

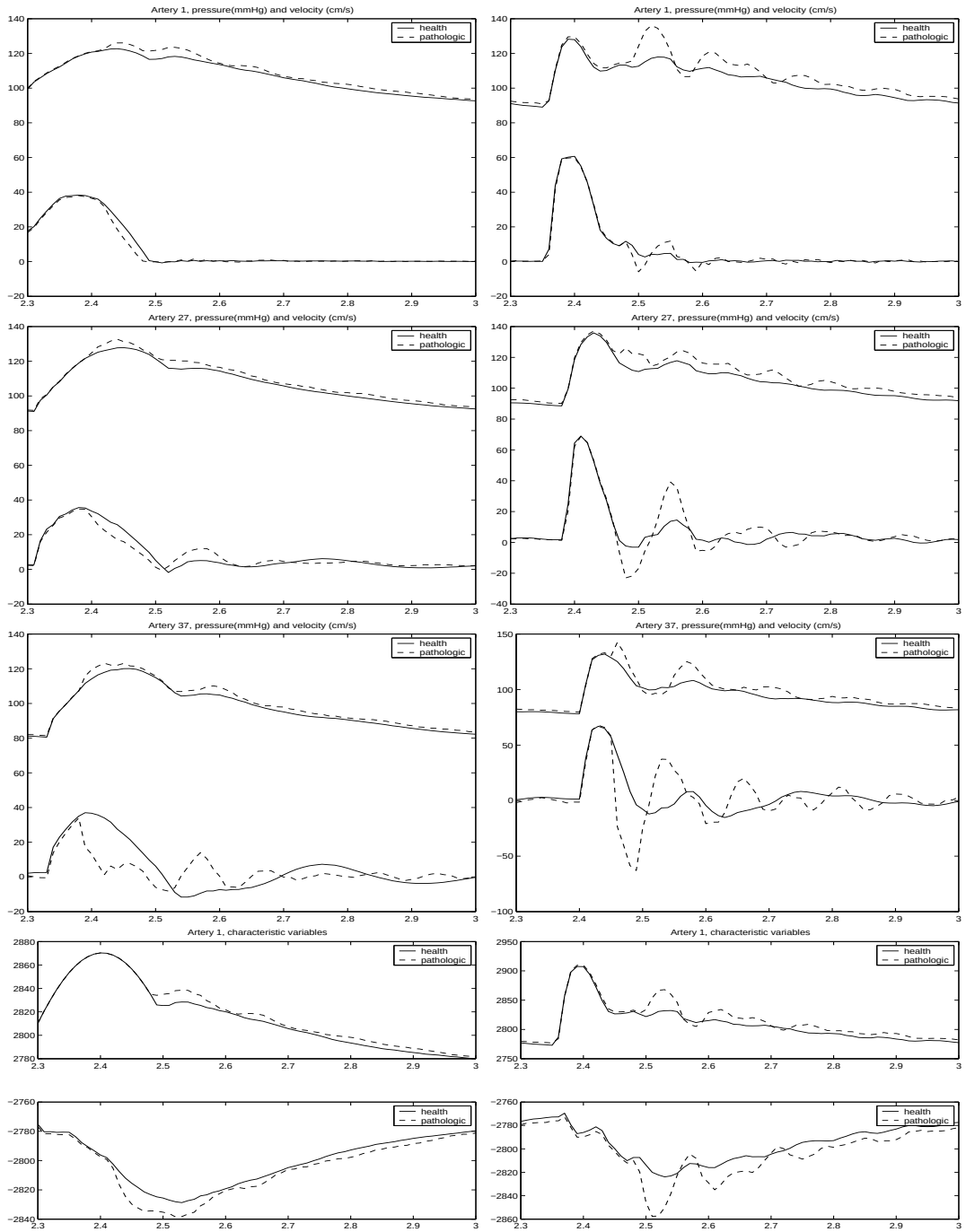

Figure 12. Comparison between the results obtained with standard proximal conditions (left) and the coupling with the ventricular model (right). Values of velocity and pressure in the mid-point of selected arteries are presented in the first three rows. The last two rows illustrate a comparison between the Riemann invariants W_1 and W_2, respectively. We have simulated adult circulation in a physiologic (solid) and pathologic (dotted) test case.

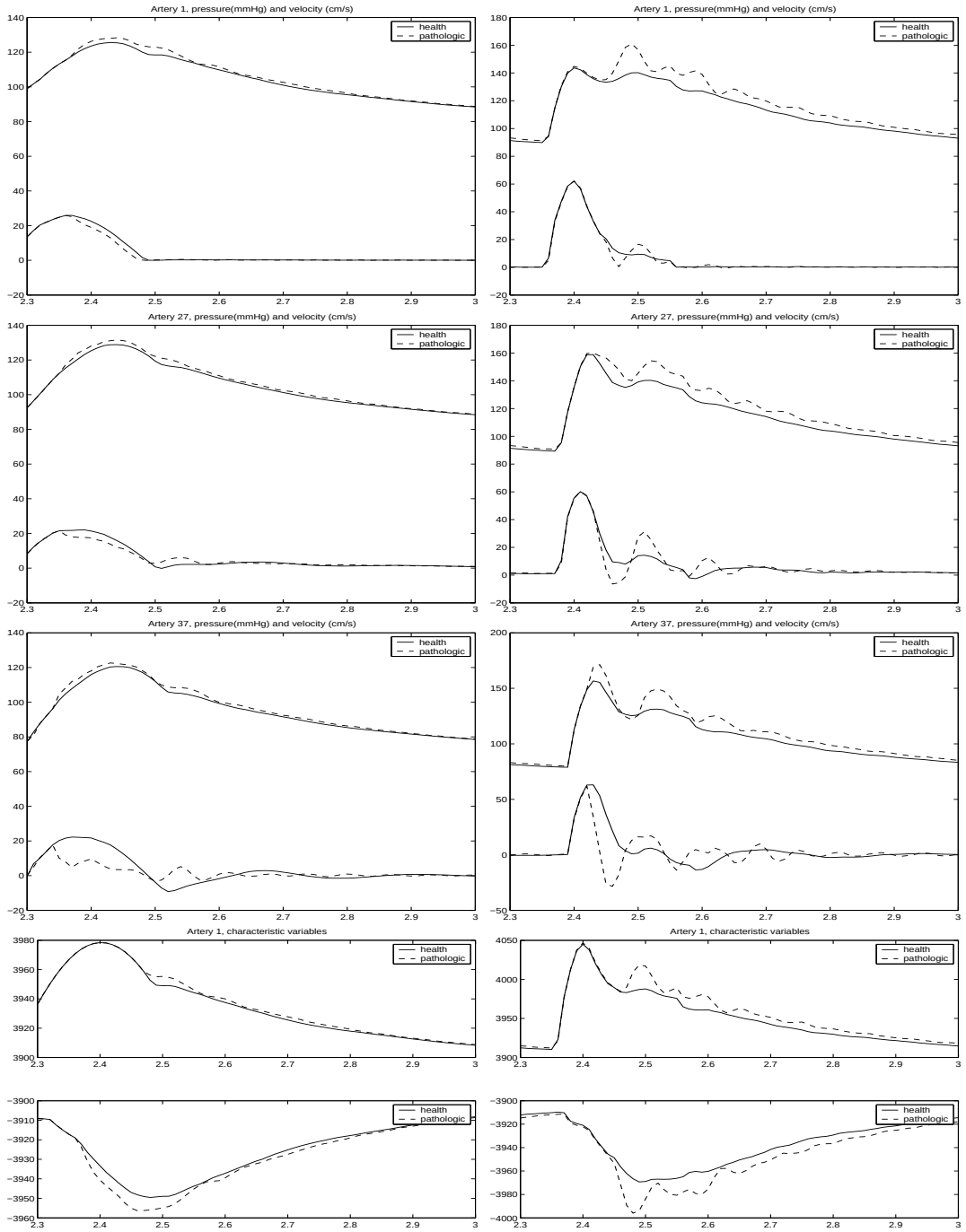

Figure 13. Same simulation of Fig.12 for an elder individual.

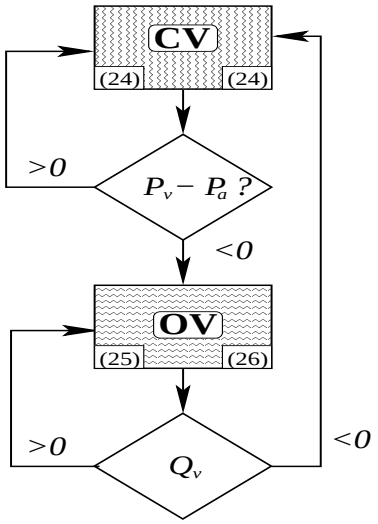

Figure 9. Flow chart representation of the aortic valve modeling. The numbers inside the boxes refer to the corresponding conditions in the text. Numbers on the left hand side refer to standard treatment, on the right hand side to the coupling with a lumped parameters model for the heart.

4. Numerical tests and results

In our simulations we start from the basic arterial network depicted in Fig. 10. In each of its 55 arterial segments, we assume Eqns. (1, 2) to hold, while bifurcations are described by (11). The values of the physical parameters (lengths, rest radii, Young moduli, etc.) have been taken from [34] and are reported in Tab. 3.4. In the same work suitable values for the distal impedances are provided and have bee adopted in this work for the *physiological* test cases. The same network has been used in [34], [24] and [25].

Here, we will compare the results obtained with the standard boundary conditions for the heart against the proposed coupled model. In the former, when the aortic valve is open P_v is prescribed to be a half-sinus curve, as pointed out in Sect. 2.2.2 (see Fig. 7).

We have considered two different scenarios, in order to assess the correctness of the numerical model.

Age effects. We have modified the artery characteristics to account for different ages. More precisely, the Young modulus has been reduced by half in the case of an adolescent individual and doubled for an elder.

Pathological case. In order to outline the on-rise of wave reflections caused by pathologies, we considered the case of a complete obstruction of the right femoral artery. This means that in this case the network reduces to a set of 53 vessels, as indicated in Fig.11, and the distal conditions on the right femoral artery corresponds to a complete blockage (i.e. $R_T = 1$). In the sequel, simulations referring to network of Fig. 11 will be denoted as *pathological*.

In Fig.12 we report the results for a middle aged individual and compare results obtained within the standard treatment of proximal boundary conditions (left column) and with the left ventricle coupling (right column). In particular, we illustrate the pressure and the velocity of blood for different arteries of the system. The last two pictures in each column refer to the Riemann invariants (W_1 and W_2 respectively) computed for the same simulations. Both the physi-

ological and the pathological network have been considered. Fig. 13 refers to the same simulation carried out in the case of an elder individual.

The next simulations have been obtained with the left-ventricle coupling exclusively.

Fig.14, 15, 16, 17 and 18 refer to simulations of the physiological case. In particular, Figure 14 shows the behaviour of the arterial pressure and flow waves in arteries at different locations of the system in the physiological case, for a middle aged individual. We report results from the thoracic aorta up to the tibial artery.

Figure 15 compares the behaviour of the arterial pressure and flow waves in arteries of subjects of different ages, while in Fig. 16 we report the evolution of the ventricular pressure and the aortic pressure during a heart beat (left) and the Pressure-Volume curves for the heart for a middle aged and an elderly patient. It is worth pointing out that this curves refer to the diagram $P - V$ only during the systolic phase, when the arterial network and the heart are in fact interacting.

The Figure 17 shows the behaviour of the pressure wave forms as a function of location from the ascending aorta to the iliac bifurcation compared with the flow wave pattern in each chosen artery.

Fig.18 shows the behaviour of subclavian artery pressure wave compared to that of aortic arch for a middle aged individual.

Finally, Fig. 19 compares the results of the physiological and the pathological cases. More precisely, we report the different behaviour of the abdominal aorta pressure waves.

5. Discussion

Physiopathological evidence suggests that major differences in the shape of aortic flow and pressure waves among patients occur either in the presence or in the absence of cardiovascular diseases [13,14]. In fact, the contour of pressure and flow waves in major systemic arteries can be basically explained on the basis of wave reflections and their interaction with the heart. The physical structure of the arterial system leads indeed to the reflection of waves at critical regions such as bifurcations, abrupt changes of the arterial stiffness or radius. These reflections are by far relevant in determining the working point of the coupled heart/arterial network system (see [15]).

The model presented here is able to describe both the left-ventricle/arterial system coupling and the wave reflections arising at the critical regions.

Impact of the heart coupling in the numerical results

The impact of the coupling of the heart in the numerical model is evident from Fig. 12 and 13. In particular, it is worth to mention that the standard (uncoupled) treatment of proximal boundary conditions underestimates the reflections in the pathological case. This was to be expected, since in the non-coupled case the action of the heart is actually independent of the real overload induced on the heart by the increasing of the peripheral resistances. This induces a sort of smoothing effect, that strongly damps the wave reflections. In particular, looking at the Riemann invariants, in the non-coupled case the incoming variable W_1 is obviously independent of the outgoing waves, which is however unphysical. On the other hand, the presence of wave reflections is felt by the heart in the coupled model.

Another remark refers to Fig. 13, where an elder is considered. The sensitivity to the variation of arterial stiffness of the model using standard proximal conditions is significantly lower than in the coupled model, as can be noticed by comparing the results obtained for a middle aged individual. The former results appear to be more in line with what expected.

These results show the relevance of the heart coupling.

Behaviour of the pressure/flow waves along the arterial tree

From Fig. 14 it is possible to see how the numerical model is able to correctly simulate the behaviour of arterial flow and pressure waves as they travel away from the heart. As shown in the figure, mean pressure falls slowly but the pulsating pressure variation increases up to the tibial artery. It may double that at the root of the aorta. The flow oscillation, on the contrary, diminishes markedly from proximal aorta to tibial arteries. Such behaviour can only be accounted

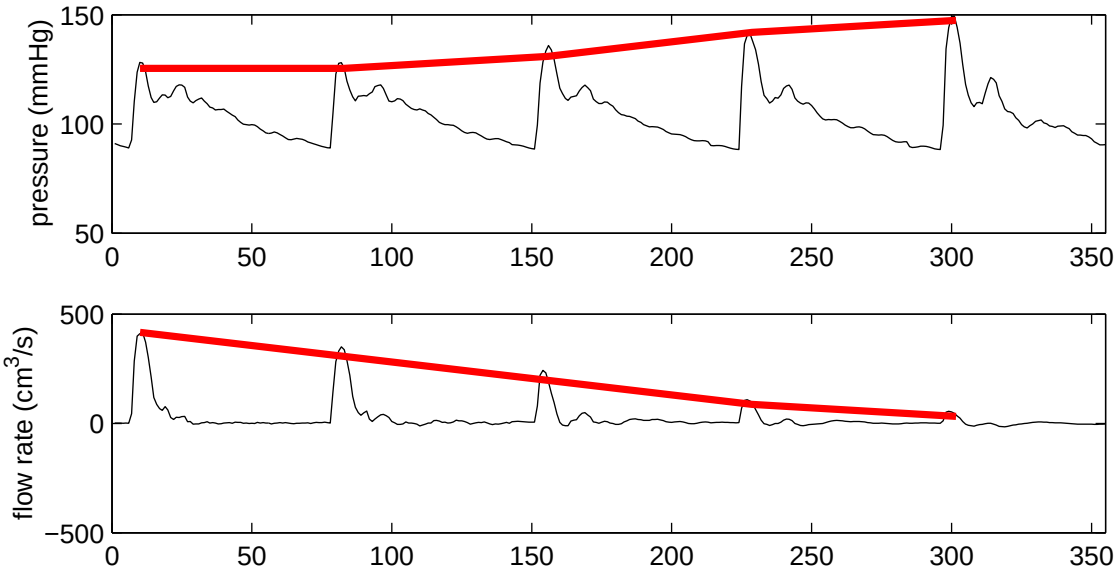

Figure 14. Snapshot of flow and pressure variation along the aorta up to the tibial artery. The thick line highlights the variation of the peak values.

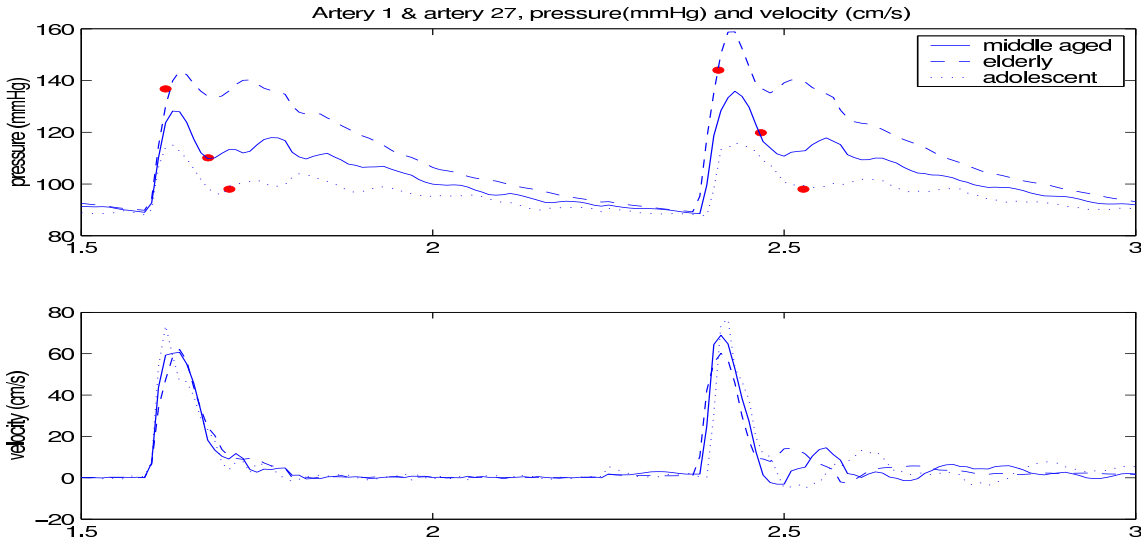

Figure 15. Time history of pressure and flow in the ascending (top) and thoracic (bottom) aorta for different aged individuals. Physiological case.

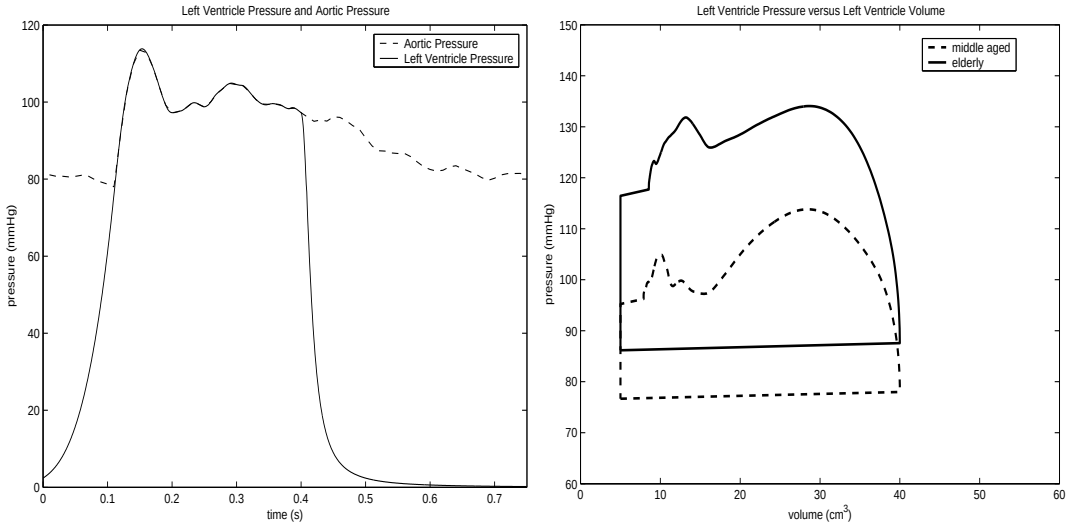

Figure 16. Time history of the left ventricle and aortic pressures during a heart beat (left) and pressure-volumes diagrams for the left ventricle (systolic phase only) in a middle-aged and an elder individual (right).

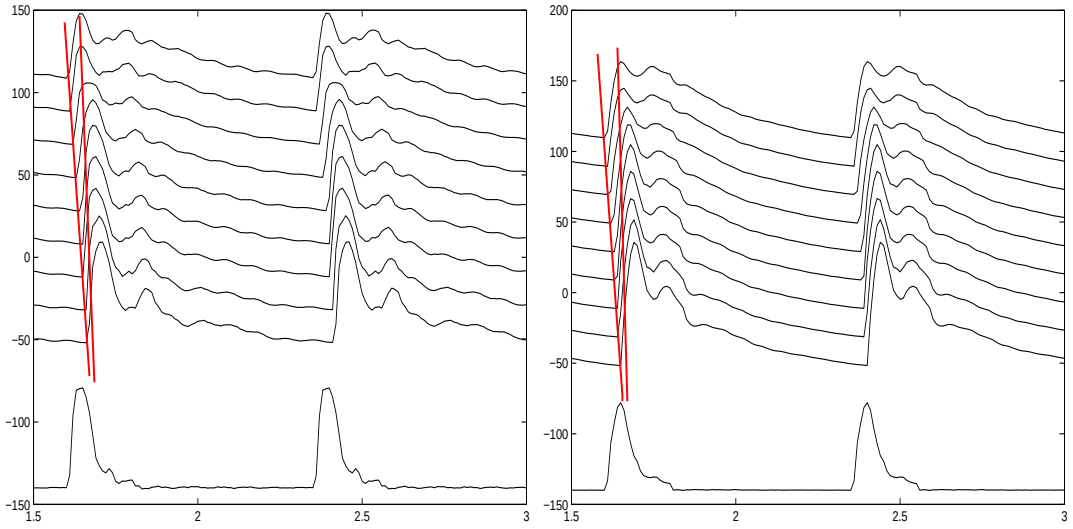

Figure 17. Pressure waves at different locations (from ascending aorta to iliac bifurcation) for a middle aged (left) and an elderly patient (right). On the bottom we report the flow rate in the ascending aorta.

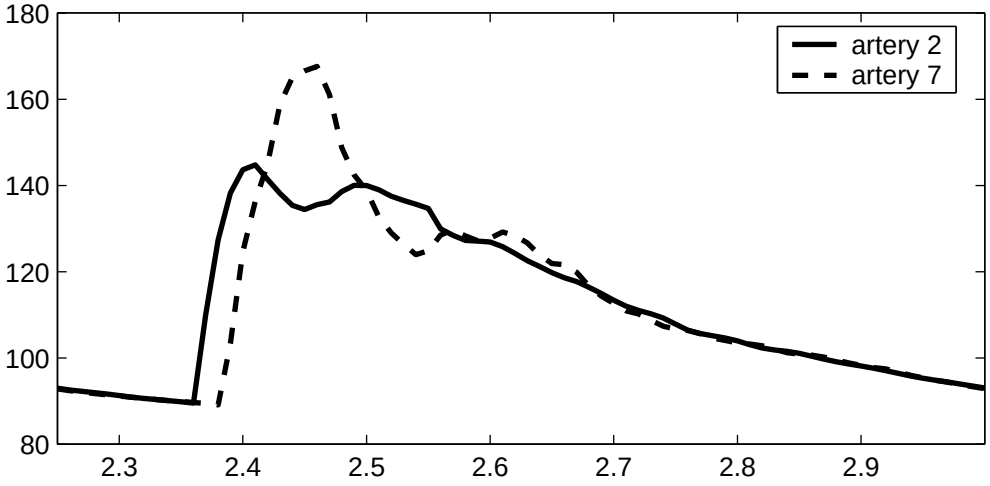

Figure 18. Results of the physiological test case in the aortic arch and in the subclavian artery.

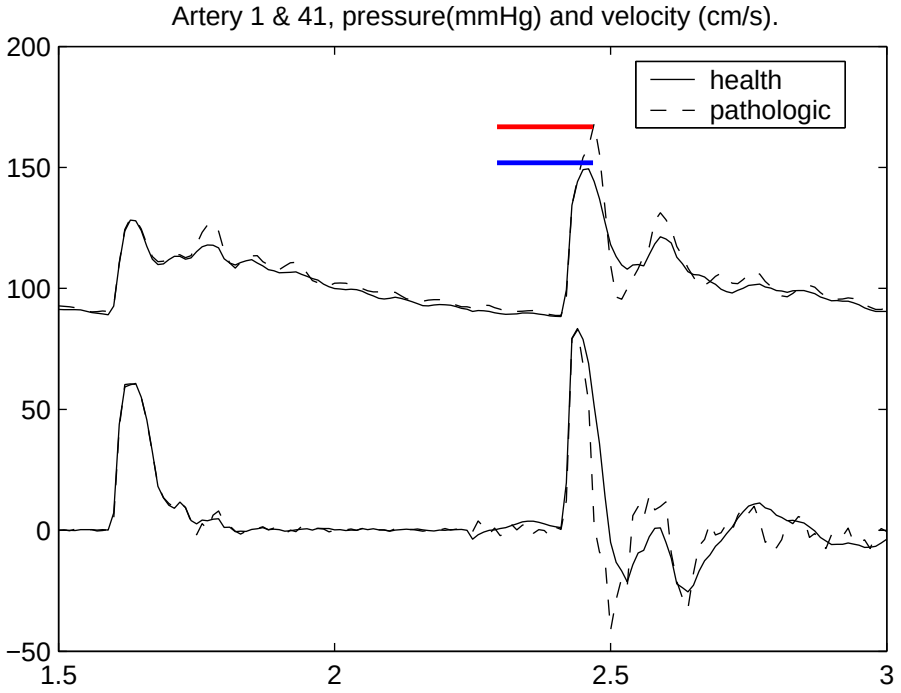

Figure 19. Ascending (top) and abdominal (bottom) pressure waves for the physiological and the pathological cases.

for by the presence of a strong reflection in the small peripheral vessels, due to high peripheral resistances. In fact, in the absence of reflections (low peripheral resistances) damping would cause a parallel fall in pressure and flow oscillations. The region of this fall seems to be the smallest arteries and proximal arterioles as well as the splanchnic branches of the abdominal aorta (renal, superior and inferior mesenteric). Yet in the latter case there is no back flow and the flow contour is similar to that of pressure. This can be attributed to low peripheral resistance and to a low reflection coefficient in vascular beds supplied by these arteries (see [12], [14]).

Ageing effects

In Fig. 15 it is evident that the system is able to simulate the major changes of the arterial pulse as seen with hypertension or ageing. Usually these alterations are attributable to arterial stiffening and to the higher speed of pulse waves along the major arteries, and the consequent early return of wave reflection from the periphery of the body. Comparing flow and pressure waves, one notes that in the young adult the wave speed is low and reflections arrive late, i.e. they arrive in diastole back in the aorta. In the older individual wave speed has increased and the reflections return in systole. This is the reason for disappearance of the reflected wave from diastole and its movement into systole, with the characteristic boost of late systolic pressure in elderly patients. Decreased compliance per se also increases pressure wave amplitude. Increased wave velocity causes wave reflection to return earlier and often leads to fusion of incident and reflected waves with generation of a pressure wave with a later systolic peak in all major arteries. It is worth noting that the increase of the arterial stiffness induces a heart overload. This can be seen in the $P - V$ diagrams on the right of Fig. 16. The increment of the area spanned by the $P - V$ curve is evident and corresponds to the ventricular overload induced by stiffening.

The appearance of reflected waves is outlined also in Fig. 17 where it occurs progressively earlier in systole as the wave approaches the iliac bifurcation. The amplitude of the reflection increases peripherally. As previously pointed out, the morphology of the network induces the presence of reflections. Possible reflecting sites include branching points, a change of arterial calibre (tapering), or of the elastic properties of the arterial wall [12]. At a given location in the ascending aorta the forward pulse wave interacts with the backward travelling (reflected) wave while systole is still in progress. This reflected wave "adds up" to the forward wave and yields the archetypal ascending aorta pressure wave-form [14]. The interaction with the reflected wave, as indicated by comparing flow and pressure waves, occurs progressively earlier in systole as we approach the iliac bifurcation. As the initial portion of the reflected wave occurs progressively early during the systole with increasing distance from the aortic valve, the diastolic portion of the reflected wave moves from diastole into systole too. In addition to the earlier appearance of the reflected wave, the amplitude of the reflection increases peripherally. These observations further support the evidence that the terminal abdominal aorta behaves as the major reflection site in man[14] (see Fig.17).

Circulation in the upper body

Arterial terminations in the upper part of the body are another relevant reflecting site. As a matter of fact, in man peak and nadir of the brachial artery pressure waves are considered to represent systolic and diastolic pressure throughout the whole arterial system. Moreover, the contour of pressure pulse in the upper limb is quite different from that in the femoral artery and its peripheral branches. For instance, there are usually two systolic peaks in the brachial artery but only one in the femoral artery. This suggest a sort of amplification in the upper limb arteries due to the shortest time period between the initial systolic peak and diastolic wave (see Fig. 20). In normal circumstances the arterial pressure wave is markedly amplified in transit from the ascending aorta to the radial artery [2]. Moreover, when arterial pressure is taken on the upper arm by using a sphygmomanometer, we actually measure the pressure in the brachial artery, which is different from the pressure in the aorta (or other

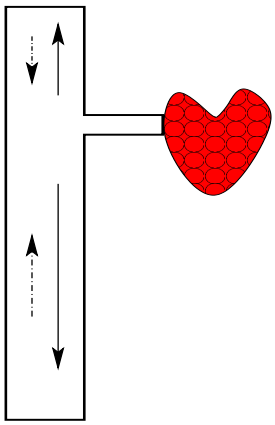

Figure 20. Representation of the arterial system, pinpointing the difference between upper and lower parts of the circulation, at the basis of the different pressure wave behaviour (see [15]).

distributing arteries) [17]. Our system is able to simulate this amplification phenomenon in the brachial artery due to the shortest time period between the initial systolic peak and the diastolic wave. In normal situations this difference may be relatively small in absolute terms and may warrant the assumption that central aortic and brachial systolic pressures are identical.

Pathological case
Finally, in Fig. 19, it can be noticed that arterial obstruction causes little perceptible changes in flow and pressure wave contours of the proximal aorta, while flow and pressure wave contours are markedly altered in the diseased artery. This can be explained by dissipation phenomenons from abdominal to thoracic aorta. When the obstruction is at a distance, the net effect to the flow is similar to that seen during peripheral vasoconstriction, with a fall in the entire flow with the onset of a back flow. Arterial obstruction is associated to a decrease in amplification of the pressure wave as a result of a local higher reflection phenomenon. Local aortic systolic pressure in presence of iliac-femoral artery obstruction may exceed the normal aortic pressure by far 30-50 mm Hg.

5.1. Conclusions and Future Developments

In this paper we have presented a novel approach for the simulation of the arterial network with a low computational costs. Specific attention has been devoted to the coupling between the left ventricle and the arterial system, as it physio-pathological relevance is well known.

The mathematical model have given good results in the several numerical tests we have performed, where it has demonstrated to be able to describe the relevant features of pressure wave propagation and reflections within the arterial system.

Future developments will be devoted to further applications of the model to simulation of pathological cases, in particular the simulation of wave reflections induced by the presence endoprosthesis or by surgical operations such as the insertion of a by-pass.

From the modelling viewpoint, a next improvements will be the inclusion of the venous system together with a more precise description of the heart functioning, starting form the ideas proposed in [23], possibly extended to include the electric activation of the myocardium.

REFERENCES

1. D. Ambrosi and L. Quartapelle. A Taylor-Galerkin method for simulating nonlinear dispersive water waves. *J. Comput. Phys.*, 146(2):546–569, 1998.
2. G.R. Cokelet. The rheology and tube flow of blood. In R.Skalak and S. Chen, editors, *Handbook of Bioengineering*. McGraw-Hill, 1987.
3. J. Donea, S. Giuliani, H. Laval, and L. Quartapelle. Time-accurate solutions of advection-diffusion problems by finite elements. *Comp. Meth. Appl. Mech. Engng.*, 45:123–145, 1984.
4. L. Euler. *Principia pro motu sanguinis per arterias determinando*, volume 2, chapter Opera posthuma mathematica et physica

anno 1844 detecta, pages 814–823. ediderunt Ph Fuss et N Fuss Petropoli, Appund Eggers et Socios, 1844.

5. C. Peskin F. Hoppensteadt. *Mathematics in Life SCiences and Medicine*. Springer-Verlag, New York, 1992.
6. L. Formaggia, D. Lamponi, and A. Quarteroni. One dimensional models for blood flow in arteries. *J Eng Math*, 47:251–276, 2003.
7. L. Formaggia, F. Nobile, and A. Quarteroni. A one dimensional model for blood flow: application to vascular prosthesis. In I. Babuska, T. Miyoshi, and P.G. Ciarlet, editors, *Mathematical Modeling and Numerical Simulation in Continuum Mechanics*, volume 19 of *Lecture Notes in Computational Science and Engineering*, pages 137–153, Berlin, 2002. Springer-Verlag.
8. L. Formaggia, F. Nobile, A. Quarteroni, and A. Veneziani. Multiscale modelling of the circulatory system: a preliminary analysis. *Computing and Visualisation in Science*, 2:75–83, 1999.
9. L. Formaggia and A. Veneziani. *Reduced and Multiscale Models for the Human Cardiovascular System*, chapter Lecture Notes of the 7^{th} VKI Lecture Series, "Biological Fluid Dynamics". Von Karman Institute, 2003.
10. E. Godlewski and P.-A. Raviart. *Numerical Approximation of Hyperbolic Systems of Conservation Laws*, volume 118 of *Applied Mathematical Sciences*. Springer, New York, 1996.
11. J. Keener and J. Sneyd. *Mathematical Physiology*. Interdisciplinary Applied Mathematics - Springer NY, 1998.
12. R.D. Latham, N. Westerhof, P. Sipkema, B. Rubal, and P. Reuderink. Regional wave travel and reflections along the human aorta: a study with six simultaneous micromanometric pressures. *Circulation*, 72:1257–1269, 1985.
13. J. Murgo, S.A. Altobelli, J.F. Dorethy, J.R. Logsdon, and G.M. McGranathan. Normal ventricular ejections dynamics in man during rest and exercis. In D.F. Leon and J.A. Shaver, editors, *Physiologic Principles of heart sounds and murmurs*, pages 92–. American Heart Association, Dallas, 1975.
14. J.P. Murgo, N. Westerhof, J.P. Giolma, and S.A. Altobelli. Aortic impedance in normal man: relationship to pressure waveforms. *Circulation*, 62:105–116, 1980.
15. W.W. Nichols and M.F. O'Rourke. *McDonald's Blood Flow in Arteries*. Edward Arnold, London, fourth edition, 1998.
16. M. Olufsen. *Modeling the arterial system with reference to an anestesia simulator*. PhD thesis, Rotskilde Univ., 1998. Tekst 345.
17. M.F. O'Rourke, A.P. Avolio, and W.W. Nichols. Left ventricular systemic arterial coupling in humans and strategies to improve coupling in disease states. In F.C.P. Yin, editor, *Vascular/Ventricular coupling.*, pages 1–19. Spring Publishing Co, Inc., New York, 1987.
18. T.J. Pedley. *The Fluid Mechanics of Large Blood Vessels*. Cambridge University Press, Cambridge, G.B., 1980.
19. F. Phythoud, N. Stergiopulos, and J.-J. Meister. Forward and backward waves in the arterial system: nonlinear separation using Riemann invariants. *Technology and Health Care*, 3:201–207, 1995.
20. A. Quarteroni and L. Formaggia. Mathematical modelling and numerical simulation of the cardiovascular system. In N. Ayache (Guest), P.G. Ciarlet, and J.L. Lions, editors, *Modelling of Living Systems*, Handbook of Numerical Analysis. Elsevier Science, Amsterdam, 2003. to appear.
21. A. Quarteroni and A. Valli. *Numerical Approximation of Partial Differential Equations*. Springer-Verlag, Berlin, 1994.
22. P. Segers, P. Morimont, P. Kohl, N. Stergiopulos, N. Wetserhof, and P. Verdonck. Arterial elastance and heart-arterial coupling in aortic regurgitation are determined by aortic leak severity. *Am. Heart J.*, 568-576, 2002.
23. P. Segers, N. Stergiopulos, N. Westerhof, P. Wouters, P. Kolh, and P. Verdonck. Systemic and pulmonary hemodynamics assessed with a lumped-parameter heart-arterial interaction model. *J. Eng. Math.*, 47:185–199, 2003.
24. S.J. Sherwin, L. Formaggia, J. Peiró, and

V. Franke. Computational modelling of 1D blood flow with variable mechanical properties and its application to the simulation of wave propagation in the human arterial system. *Int. J. Numer. Meth. Fluids*, 43:673–700, 2003.

25. S.J. Sherwin, V. Franke, J. Peiró, and K. Parker. One-dimensional modelling of a vascular network in space-time variables. *J Eng. Math.*, 47:217–250, 2003.
26. F.T. Smith, N.C. Ovenden, Franke P.T., and Doorly D.J. What happens to pressure when a flow enters a side branch? *Journal of Fluid Mechanics*, 479:231–258, 2003.
27. N.P. Smith, A.J. Pullan, and P.J. Hunter. An anatomically based model of coronary blood flow and myocardial mechanics. *SIAM J. Appl. Math.*, 62(3):990–1018, 2002.
28. N Stergipulos and D.F. Young. Computer simulation of arterial flow with applications to arterial and aortic stenoses. *J. Biomech.*, 25(12):1477–1488, 1992.
29. J.C. Stettler, P. Niederer, and M. Anliker. Theoretical analysis of arterial hemodynamics including the influence of bifurcations, part i: Mathematical model and prediction of normal pulse patterns. *Annals of Biomedical Engineering*, 9:145–164, 1981.
30. V.L. Streeter, W.F. Keitzer, and D.F. Bohr. Pulsatile pressure and flow through distensible vessels. *Circulation Research*, 13:3, 1963.
31. H. Suga and K. Sagawa. Instantaneous pressure-volume relationships and their ratio in the excised supported canine left ventricle. *Circ. Res.*, 35:117–126, 1974.
32. H. Suga, K. Sagawa, and A.A. Shoukas. Load independence of the instantaneous pressure-volume ratio of the canine left ventricle and effects of epinephrine and heart rate on the ratio. *Circ. Res.*, 32:314–322, 1973.
33. S. Čanić. Blood flow through compliant vessels after endovascular repair: wall deformations induced by the discontinuous wall properties. *Computing and Visualisation in Science*, 4, 3:147–155, 2002.
34. J.J. Wang and K. Parker. Wave propagation in a model for arterial circulation. to appear in J. Biomech, 2004.
35. N. Westerhof, F. Bosman, C. Vries, and A. Noordergraaf. Analog studies of the human systemic arterial tree. *J. of Biomech*, 2:121–143, 1969.